TÜBİTAK

Turkish Journal of Mathematics

http://journals.tubitak.gov.tr/math/

Research Article

Turk J Math
(2017) 41: 1027 – 1041

doi:10.3906/mat-1602-38

Finite volume approximation of the relativistic Burgers equation on a Schwarzschild–(anti-)de Sitter spacetime

Tuba CEYLAN[1], **Baver OKUTMUŞTUR**[2,*]
[1]Central Bank of the Republic of Turkey, Ankara, Turkey (TCMB)
[2]Department of Mathematics, Middle East Technical University, Ankara, Turkey

Received: 11.02.2016 • **Accepted/Published Online:** 17.10.2016 • **Final Version:** 25.07.2017

Abstract: The relativistic versions of Burgers equations on the Schwarzschild, FLRW, and de Sitter backgrounds have recently been derived and analyzed numerically via finite volume approximation based on the concerned models. In this work, we derive the relativistic Burgers equation on a Schwarzschild–(anti-)de Sitter spacetime and introduce a second-order Godunov-type finite volume scheme for the approximation of discontinuous solutions to the model of interest. The effect of the cosmological constant is also taken into account both theoretically and numerically. The efficiency of the method for solutions containing shock and rarefaction waves are presented by several numerical experiments.

Key words: Relativistic Burgers equation, spacetime, Schwarzschild–de Sitter metric, Schwarzschild–de Sitter background, finite volume method, Godunov scheme

1. Introduction

The theory of derivation of relativistic-type Burgers equations on curved spacetimes was initiated by LeFloch et al. [6] and developed together with collaborators [2–4]. In particular, the first model of interest, which may be considered as the fundamental relativistic Burgers equation, was derived in different ways, either from the Euler system on a curved background or by introducing a hyperbolic balance law on a flat background carrying out the same Lorentz invariance property fulfilled by the Euler equations of relativistic compressible fluids. This analysis has recently been extended to the Schwarzschild, Friedmann–Lemaitre–Robertson–Walker (FLRW), de Sitter, and anti-de Sitter spacetimes and studied numerically by means of finite volume approximation [2–4, 6].

In this paper we are interested in compressible fluids developing on a curved spacetime, particularly on the domain of a Schwarzschild–(anti-)de Sitter geometry. The fluid flows under consideration may include shock waves and we study within a class of weak solutions to the Euler equations on the concerned geometry. Throughout this article, we denote the Schwarzschild–de Sitter and Schwarzschild–anti-de Sitter spacetimes by SdS and SAdS spacetimes, respectively. Representing the Levi-Civita connection associated with the SdS–SAdS metric by ∇, the Euler equations for a compressible fluid on a curved spacetime are formularized as

$$\nabla_\alpha\big(T^{\alpha\beta}(\rho,u)\big)=0, \tag{1.1}$$

where the energy-momentum tensor of perfect fluids given by

$$T^{\alpha\beta}(\rho,u)=\rho c^2u^\alpha u^\beta+p(\rho)\big(u^\alpha u^\beta+g^{\alpha\beta}\big) \tag{1.2}$$

*Correspondence: baver@metu.edu.tr

is based on the mass-energy density of the fluid $\rho \geq 0$ and its velocity field $u = (u^\alpha)$. Here, $c > 0$ is the light speed, p is the pressure stated as a function $p = p(\rho)$ of the mass energy density, and u^α is unit timelike vector field so that

$$u^\alpha u_\alpha = -1, \quad \text{with} \quad u^0 > 0.$$

1.1. Motivation and purpose of the paper

The inviscid Burgers equation is one of the simplest nonlinear hyperbolic conservation laws. It supplies a simple model, which permits discontinuous solutions and generates a simplified framework for shock-capturing numerical methods. The Burgers equation and its generalizations to a curved spacetime have been generally used in physical and engineering science. The classical (inviscid) Burgers equation is as follows:

$$\partial_t v + \partial_x(v^2/2) = 0,\ v = v(t,x),\ t > 0,\ x \in \mathbb{R}. \tag{1.3}$$

This equation can be deduced from the Euler system of compressible fluids:

$$\begin{aligned} &\partial_t \rho + \partial_x(\rho v) = 0, \\ &\partial_t(\rho v) + \partial_x(\rho v^2 + p(\rho)) = 0, \end{aligned} \tag{1.4}$$

in which v represents the velocity, $\rho \geq 0$ the density, and $p(\rho)$ the pressure of the fluid. Indeed, imposing $p(\rho) \equiv 0$ in system (1.4) and taking a suitable combination of both equations,

$$\begin{aligned} 0 &= v\,\partial_t(\rho) + \rho\,\partial_t(v) + v^2\partial_x(\rho) + 2v\rho\,\partial_x(v) \\ &= \rho(\partial_t v + 2v\partial_x v) + v(\partial_t \rho + v\partial_x \rho) \\ &= \rho(\partial_t v + v\partial_x v) \end{aligned}$$

gives the inviscid Burgers equation (1.3).

In the current work, we apply this analysis to derive the relativistic Euler equations on smooth, time-oriented, curved SdS–SAdS spacetimes in order to obtain the relativistic Burgers equation on these backgrounds. We are inspired by the work of LeFloch and his collaborators for the derivation of the model and we apply the strategy therein [2, 3, 6]. Similar to the nonrelativistic case, we impose zero pressure in the Euler equations (1.1) on the SdS–SAdS spacetimes to derive the relativistic Burgers equation.

The convergence and geometric formulation of finite volume schemes on a curved spacetime is based on previous articles [1, 6, 7]. The construction of the first- and second-order Godunov-type finite volume schemes was introduced in the book by Guinot [5] and the article by Van Leer [9].

The content of this article is as follows. We introduce the basic features of the SdS and SAdS geometries in Section 2. The relation between the SdS–SAdS and different spacetime metrics depending on cosmological constant Λ and mass parameter m is analyzed in this part. We then calculate the Euler equations by the help of the Christoffel symbols and energy-momentum tensor terms. After getting the pressureless Euler equations, we connect our model to the Euler equations to derive the relativistic Burgers equation on the SdS–SAdS backgrounds. In Section 3, we first present a geometric formulation of the finite volume method on a curved background and then introduce the finite volume strategy on local coordinates. Construction of the first- and second-order Godunov schemes and various numerical tests are displayed in Section 4. The effects of the cosmological constant on the numerical scheme are also examined in the numerical part. We end the article with a summary involving concluding remarks.

2. Euler equations

2.1. SdS–SAdS spacetime metric

The SdS spacetime is a spherically symmetric black hole solution to Einstein's vacuum field equations with cosmological constant Λ and its metric in terms of time t, radial r, and angular coordinates (θ and φ) is represented in spherical coordinates with signature $(-,+,+,+)$ by

$$g=-\Big(1-\frac{2m}{r}-\frac{\Lambda r^2}{3}\Big)dt^2+\Big(1-\frac{2m}{r}-\frac{\Lambda r^2}{3}\Big)^{-1}dr^2+r^2(d\theta^2+\sin^2\theta d\varphi^2), \tag{2.1}$$

where $m>0$ is the mass parameter and c is the light speed. The sign of Λ is significant for assigning the spacetime geometry; that is, the background is a SdS spacetime if $\Lambda>0$ and a SAdS spacetime if $\Lambda<0$. Here we have three important observations:

- When $\Lambda=0$, the metric (2.1) reduces to

$$g=-\Big(1-\frac{2m}{r}\Big)dt^2+\Big(1-\frac{2m}{r}\Big)^{-1}dr^2+r^2(d\theta^2+\sin^2\theta d\varphi^2), \tag{2.2}$$

  which describes a Schwarzschild metric. That is, $\Lambda=0$ corresponds to the Schwarzschild spacetime.

- If the mass parameter $m=0$, the metric (2.1) reduces to

$$g=-\Big(1-\frac{\Lambda r^2}{3}\Big)dt^2+\Big(1-\frac{\Lambda r^2}{3}\Big)^{-1}dr^2+r^2(d\theta^2+\sin^2\theta d\varphi^2), \tag{2.3}$$

  which is the de Sitter metric if $\Lambda>0$ and the anti-de Sitter metric if $\Lambda<0$. Thus, $m=0$ corresponds to the de Sitter or anti-de Sitter spacetime.

- If both the cosmological constant Λ and the mass parameter m vanish, then the metric (2.1) reduces to

$$g=-dt^2+dr^2+r^2(d\theta^2+\sin^2\theta d\varphi^2), \tag{2.4}$$

  which is the Minkowski (flat) metric, and hence it corresponds to the Minkowski (flat) spacetime.

In terms of Cartesian coordinates $x=r\sin\theta\cos\varphi$, $y=r\sin\theta\sin\varphi$, and $z=r\cos\theta$, with the indexes $(0,1,2,3)$ indicating the coordinates (t,r,θ,φ), the metric (2.1) is represented by

$$(g_{\alpha\beta})=\begin{pmatrix}-\Big(1-\frac{2m}{r}-\frac{\Lambda r^2}{3}\Big) & 0 & 0 & 0\\ 0 & \Big(1-\frac{2m}{r}-\frac{\Lambda r^2}{3}\Big)^{-1} & 0 & 0\\ 0 & 0 & r^2 & 0\\ 0 & 0 & 0 & r^2\sin^2\theta\end{pmatrix}$$

where the nonzero covariant elements are

$$g_{00}=-\Big(1-\tfrac{2m}{r}-\tfrac{\Lambda r^2}{3}\Big),\quad g_{11}=\Big(1-\tfrac{2m}{r}-\tfrac{\Lambda r^2}{3}\Big)^{-1},$$
$$g_{22}=r^2,\qquad g_{33}=r^2\sin^2\theta,$$

and the inverse $(g^{\alpha\beta})$ of $(g_{\alpha\beta})$ is

$$(g^{\alpha\beta}) = \begin{pmatrix} -\left(1-\frac{2m}{r}-\frac{\Lambda r^2}{3}\right)^{-1} & 0 & 0 & 0 \\ 0 & \left(1-\frac{2m}{r}-\frac{\Lambda r^2}{3}\right) & 0 & 0 \\ 0 & 0 & r^{-2} & 0 \\ 0 & 0 & 0 & (r^2\sin^2\theta)^{-1} \end{pmatrix}$$

where the corresponding contravariant elements are

$$g^{00} = -\left(1-\tfrac{2m}{r}-\tfrac{\Lambda r^2}{3}\right)^{-1}, \qquad g^{11} = \left(1-\tfrac{2m}{r}-\tfrac{\Lambda r^2}{3}\right),$$
$$g^{22} = \tfrac{1}{r^2}, \qquad g^{33} = \tfrac{1}{r^2\sin^2\theta}.$$

Here we have

$$g^{ik}g_{kj} = \delta^i_j = \begin{cases} 1 & \text{if } i=j, \\ 0 & \text{if } i\neq j, \end{cases}$$

with δ^i_j the Kronecker delta function.

2.2. Derivation of the Euler equations

We need to calculate each term of the Christoffel symbols $\Gamma^\mu_{\alpha\beta}$ in order to derive the Euler system for the SdS and SAdS geometries. The Christoffel symbols are formulated by

$$\Gamma^\mu_{\alpha\beta} = \frac{1}{2}g^{\mu\nu}(-\partial_\nu g_{\alpha\beta} + \partial_\beta g_{\alpha\nu} + \partial_\alpha g_{\beta\nu}), \tag{2.5}$$

where the terms $\alpha,\beta,\mu,\nu \in \{0,1,2,3\}$. A slightly long calculation shows that the terms of the Christoffel symbols are

$$\Gamma^0_{00} = 0, \quad \Gamma^0_{01} = \Gamma^0_{10} = \frac{\left(\frac{m}{r^2}-\frac{\Lambda r}{3}\right)}{\left(1-\frac{2m}{r}-\frac{\Lambda r^2}{3}\right)}, \quad \Gamma^1_{11} = \frac{\left(\frac{-m}{r^2}+\frac{\Lambda r}{3}\right)}{\left(1-\frac{2m}{r}-\frac{\Lambda r^2}{3}\right)},$$

$$\Gamma^0_{01} = \frac{\left(\frac{m}{r^2}-\frac{\Lambda r}{3}\right)}{\left(1-\frac{2m}{r}-\frac{\Lambda r^2}{3}\right)}, \qquad \Gamma^1_{00} = \left(\frac{m}{r^2}-\frac{\Lambda r}{3}\right)\left(1-\frac{2m}{r}-\frac{\Lambda r^2}{3}\right),$$

$$\Gamma^1_{22} = -r\left(1-\frac{2m}{r}-\frac{\Lambda r^2}{3}\right), \quad \Gamma^1_{33} = -r\left(1-\frac{2m}{r}-\frac{\Lambda r^2}{3}\right)\sin^2\theta,$$

$$\Gamma^2_{12} = \Gamma^2_{21} = \Gamma^3_{13} = \Gamma^3_{31} = \frac{1}{r}, \quad \Gamma^2_{33} = -\sin\theta\cos\theta, \quad \Gamma^3_{23} = \Gamma^3_{32} = \cot\theta.$$

It remains to find the energy-momentum tensors for perfect fluids in order to obtain the Euler equations. We consider our spacetime to be $(1+1)$-dimensional; that is, the solutions to the Euler system depend only on the time variable t and corresponding radial variable r, whereas the angular components θ,φ vanish. It follows that

$$(u^\alpha) = (u^0(t,r), u^1(t,r), 0, 0), \text{ with } u^\alpha u_\alpha = -1. \tag{2.6}$$

Since the velocity vector u is unit, it follows that

$$-1=-\Big(1-\frac{2m}{r}-\frac{\Lambda r^2}{3}\Big)(u^0)^2+\frac{1}{\Big(1-\frac{2m}{r}-\frac{\Lambda r^2}{3}\Big)}(u^1)^2. \tag{2.7}$$

It is suitable to introduce the scalar velocity

$$v:=\frac{c}{\Big(1-\frac{2m}{r}-\frac{\Lambda r^2}{3}\Big)}\frac{u^1}{u^0}, \tag{2.8}$$

generating

$$(u^0)^2=\frac{c^2}{\Big(1-\frac{2m}{r}-\frac{\Lambda r^2}{3}\Big)(c^2-v^2)},\quad (u^1)^2=\frac{v^2\Big(1-\frac{2m}{r}-\frac{\Lambda r^2}{3}\Big)}{(c^2-v^2)}. \tag{2.9}$$

The energy-momentum tensor components follow from (1.2) and (2.9):

$$\begin{aligned}
&T^{00}=\frac{\rho c^4+pv^2}{(c^2-v^2)\Big(1-\frac{2m}{r}-\frac{\Lambda r^2}{3}\Big)},\qquad T^{01}=T^{10}=\frac{cv(\rho c^2+p)}{(c^2-v^2)},\\
&T^{11}=\frac{c^2\Big(1-\frac{2m}{r}-\frac{\Lambda r^2}{3}\Big)(v^2\rho+p)}{(c^2-v^2)},\quad T^{22}=\frac{p}{r^2},\quad T^{33}=\frac{p}{r^2\sin^2\theta},\\
&T^{02}=T^{03}=T^{12}=T^{13}=T^{20}=T^{21}=T^{23}=T^{30}=T^{31}=T^{32}=0.
\end{aligned} \tag{2.10}$$

Then the Euler system (1.1) can be expressed in the form

$$\partial_\alpha T^{\alpha\beta}+\Gamma^\alpha_{\alpha\gamma}T^{\gamma\beta}+\Gamma^\beta_{\alpha\gamma}T^{\alpha\gamma}=0. \tag{2.11}$$

Hence, the Euler equations on the SdS–SAdS spacetimes are obtained by substituting tensor components (2.10) in equation (2.11) with repeated indices. We refer the reader to articles [2–4] for further details on tensor calculations.

2.3. Vanishing pressure Euler equations

We substitute the Christoffel symbol terms into equations (2.11) and then impose the pressure $p=0$ to obtain

$$\begin{aligned}
&\partial_0\Big(\frac{c}{(1-\frac{2m}{r}-\frac{\Lambda r^2}{3})(c^2-v^2)}\Big)+\partial_1\big(\frac{v}{c^2-v^2}\big)+\frac{v}{(c^2-v^2)}\frac{\big(-\frac{2m}{r^2}-\frac{4\Lambda r}{3}+\frac{2}{r}\big)}{\Big(1-\frac{2m}{r}-\frac{\Lambda r^2}{3}\Big)}=0,\\
&\partial_0\Big(\frac{cv}{c^2-v^2}\Big)+\partial_1\Big(\frac{v^2\big(1-\frac{2m}{r}-\frac{\Lambda r^2}{3}\big)}{c^2-v^2}\Big)+\frac{c^2}{c^2-v^2}\Big(\frac{m}{r^2}-\frac{\Lambda r}{3}\Big)\\
&+\frac{v^2}{c^2-v^2}\Big(\frac{-5m}{r^2}-\frac{\Lambda r}{3}+\frac{2}{r}\Big)=0,
\end{aligned} \tag{2.12}$$

which is called the vanishing pressure Euler equations on the SdS–SAdS backgrounds. In view of these equations, we observe the following:

- If $\Lambda = 0$, (2.12) reduces (after a suitable normalization) to the vanishing pressure Euler system on the Schwarzschild background (see [6]).
- If $m = 0$, (2.12) reduces to the vanishing pressure Euler system on the de Sitter spacetime if $\Lambda > 0$ (anti-de Sitter spacetime if $\Lambda < 0$) (see [3, 4]).
- If both $\Lambda = 0$ and $m = 0$, the system (2.12) reduces to the vanishing pressure Euler system on flat spacetime. We notice that, from the pressureless Euler system on flat spacetime, one can recover the nonrelativistic (classical) Burgers equation (see [6]).

2.4. The derivation of the model

We are motivated by the idea of recovering the relativistic Burgers equation from the pressureless Euler system on a curved background. LeFloch and his collaborators introduced the theory of this derivation in several ways and then generalized this idea for the flat, Schwarzschild, FLRW, and de Sitter geometries [2–4, 6]. In this paper we apply the same technique by taking into account the SdS–SAdS spacetimes.

To this aim, we start by rewriting the first and second equations of (2.12) with the notation $\partial_0 = \partial_t$, $\partial_1 = \partial_r$. After taking the partial derivatives of related terms in both equations of (2.12) and then keeping a convenient combination of them, we derive the following single equation:

$$\partial_t v + (1 - \frac{2m}{r} - \frac{\Lambda r^2}{3})\partial_r(\frac{v^2}{2}) = \frac{mv^2}{r^2} - \frac{\Lambda r v^2}{3} - \frac{mc^2}{r^2} + \frac{\Lambda r c^2}{3}. \tag{2.13}$$

This equation is called the relativistic Burgers equation on the SdS–SAdS spacetimes. In view of (2.13), we observe that:

- If $\Lambda = 0$, (2.13) reduces to the relativistic Burgers equation on the Schwarzschild background (see [6]).
- If $m = 0$, (2.13) reduces to the relativistic Burgers equation on the de Sitter spacetime if $\Lambda > 0$ (anti-de Sitter spacetime if $\Lambda < 0$) (see [3, 4]).
- If both $\Lambda = 0$ and $m = 0$ in (2.13), then we recover the classical (inviscid) Burgers equation

$$\partial_t v + \partial_r(v^2/2) = 0.$$

This result is coherent with the fact that the limiting case of the relativistic Burgers equations on a curved spacetime yields the classical (nonrelativistic) Burgers equation, which is a common property shared by the relativistic models.

3. Finite volume method

The finite volume method is one of the most versatile discretization techniques for scientific computing and has several applications in physical and engineering sciences. Particularly, it permits one to approximate weak solutions containing shock waves to nonlinear hyperbolic balance laws like the Euler equations of compressible fluids. The method is based on the integration of the equations over a finite volume in order to discretize the equation. In the present work, we use a finite volume approximation for general balance laws of hyperbolic partial differential equations following articles [1, 7, 8] and we apply the method to the derived relativistic Burgers equation (2.13) on a $(1+1)$-dimensional SdS(–SAdS) spacetime.

3.1. Geometric formulation

Let M be a time-oriented, $(n+1)$-dimensional curved spacetime with metric g. The geometry is time-oriented in the sense that we can distinguish between past-oriented and future-oriented vectors. We consider a hyperbolic balance law given by

$$div\big(T(v)\big) = S(v), \quad v : M \to \mathbb{R}, \tag{3.1}$$

where v is a scalar field, $div(\cdot)$ is the divergence operator, $T(v)$ is the flux vector field, and $S(v)$ is the scalar field. We seek a formulation of the finite volume scheme for discretizing (3.1) on M following Amorim et al. [1].

In general relativity, it is a usual assumption that the spacetime should be globally hyperbolic; that is, we assume that M is globally hyperbolic in the sense that M admits a foliation by spacelike, oriented hypersurfaces H_t so that

$$M = \bigcup_{t\in\mathbb{R}} H_t,$$

where each slice has the topology of a smooth n-dimensional manifold with a boundary and the hypersurface H_0 is an initial slice. We introduce a triangulation of spacetime M by

$$T^h = \bigcup_{K\in\mathcal{T}^h} K,$$

which is a collection of finite elements K satisfying the following properties:

- The boundary ∂K of an element K is piecewise smooth, n-dimensional manifold, and given by $\partial K = \bigcup_{e\subset\partial K} e$ and it contains exactly two spacelike faces represented by e_K^+ and e_K^-, and "timelike" elements, represented by
$$e^0 \in \partial^0 K := \partial K \setminus \{e_K^+, e_K^-\}.$$
- The intersection $K \cap K'$ of two distinct elements $K, K' \in T^h$ is either a common face of K, K' or else is a submanifold that has at most $(n-1)$ dimensions.
- $H_0 \subset \bigcup_{K\in\mathcal{T}^h} \partial K$, where H_0 is the initial slice.
- $|K|$, $|e_K^+|$, $|e_K^-|$, $|e^0|$ represent the measures of K, e_K^+, e_K^-, e^0, respectively, defined from the Lorentzian metric or the induced metric on these hypersurfaces.
- Along the timelike faces e_K^+, e_K^-, we define the outgoing unit normal vector field denoted by n_K.

The most natural way of establishing the finite volume method is to average the balanced law (3.1) over each element $K \in \mathcal{T}^h$ of the triangulation. We first consider the discrete solution as defined on the spacelike elements e_K^+, e_K^-. Next, to a particular element K we introduce two values, v_K^+ and v_K^-, to the unique outflow and inflow elements e_K^+, e_K^-, respectively. It follows that the value v_K of the discrete solution on the element K is the solution v_K^+ set on the outflow element e_K^+, or v_K is the solution v_K^+ set on inflow element e_K^-, or some average of the both, depending on the coherent selection throughout the background geometry.

Then the finite volume scheme follows by first integrating (3.1) for any element K in space and time, applying the divergence theorem by decomposing the boundary ∂K into its parts e_K^+, e_K^- and $\partial^0 K$, and finally

averaging the space and time elements via convenient approximations. For the finite volume scheme and further details, we refer the reader to articles [1, 6–8].

3.2. Finite volume schemes in coordinates

We work on a $(1+1)$-dimensional spacetime M, i.e. we take $n=1$ in the geometric formulation of the finite volume method. It follows that the balance law (3.1) becomes

$$\partial_t T^0(t,r) + \partial_r T^1(t,r) = S(t,r), \tag{3.2}$$

where T^0, T^1 are flux fields and S is the source term. The finite volume method is considered over each grid cell:

$$[t_n, t_{n+1}] \times [r_{j-1/2}, r_{j+1/2}].$$

Integrating (3.2) over these grid cells and introducing the approximations of the numerical flux functions gives the finite volume scheme in coordinates. We refer the reader to previous works [2–4, 6] for the formulation of finite volume schemes on a $(1+1)$-dimensional spacetime.

4. Godunov-type schemes and numerical tests

The Godunov-type finite volume scheme, which is a conservative numerical scheme, is a part of the family of shock-capturing schemes in numerical analysis and computational fluid dynamics for solving partial differential equations. In this section we introduce both first- and second-order Godunov-type schemes and numerically analyze our model (2.13) by means of these schemes with several illustrations.

4.1. First-order Godunov scheme

This part is devoted to introducing a first-order Godunov-type scheme and its illustration by numerical experiments for the derived equation attained on the SdS and SAdS geometries. Our model of interest (2.13) is examined with a single shock and rarefaction for an initial function considering the Godunov-type scheme with a local Riemann problem on each grid cell. It is a fact that in Riemann problems both shocks and rarefaction waves are produced; therefore, we look for the fastest wave at each grid cell.

The formulation of the first-order Godunov schemes is given below. We start by a normalization (imposing $c=1$) for equation (2.13), which yields

$$\partial_t v + (1 - \frac{2m}{r} - \frac{\Lambda r^2}{3})\partial_r(\frac{v^2}{2}) = \frac{mv^2}{r^2} - \frac{\Lambda r v^2}{3} - \frac{m}{r^2} + \frac{\Lambda r}{3}, \tag{4.1}$$

and the corresponding finite volume scheme is given by

$$v_j^{n+1} = v_j^n - \frac{\Delta t}{\Delta r}(b_{j+1/2}^n \, g_{j+1/2}^n - b_{j-1/2}^n g_{j-1/2}^n) + \Delta t S_j^n, \tag{4.2}$$

where the source term is

$$S_j^n = \frac{m(v_j^n)^2}{(r_j^n)^2} - \frac{\Lambda r_j^n (v_j^n)^2}{3} - \frac{m}{(r_j^n)^2} + \frac{\Lambda r_j^n}{3},$$

and the other terms in (4.2) are

$$b^n_{j\pm1/2} = 1 - \frac{2m}{(r^n_{j\pm1/2})} - \frac{\Lambda(r^n_{j\pm1/2})^2}{3},$$
$$g^n_{j-1/2} = f(v^n_{j-1}, v^n_j), \quad g^n_{j+1/2} = f(v^n_j, v^n_{j+1}),$$

with the flux function $f(u,v)$ described as follows:

$$f(u,v) = \begin{cases} \frac{u^2}{2}, & \text{if} \quad u > v \quad \text{and} \quad u+v>0, \\ \frac{v^2}{2}, & \text{if} \quad u > v \quad \text{and} \quad u+v<0, \\ \frac{u^2}{2}, & \text{if} \quad u \le v \quad \text{and} \quad u>0, \\ \frac{v^2}{2}, & \text{if} \quad u \le v \quad \text{and} \quad v<0, \\ 0, & \text{if} \quad u \le v \quad \text{and} \quad u \le 0 \le v. \end{cases} \tag{4.3}$$

It can be easily deduced that the speed term is

$$1 - \frac{2m}{(r^n_{j\pm1/2})} - \frac{\Lambda(r^n_{j\pm1/2})^2}{3}. \tag{4.4}$$

Moreover, in order to satisfy the stability condition in the scheme, we choose Δt and Δr so that

$$\frac{\Delta t}{\Delta r}\max_j\Big|1 - \frac{2m}{(r^n_{j\pm1/2})} - \frac{\Lambda(r^n_{j\pm1/2})^2}{3}\Big| \le 1.$$

The numerical tests for the first-order Godunov schemes are illustrated in Figures 1 and 2, representing shock and rarefaction wave propagations, respectively. Each of these figures consists of four subfigures displaying the time evolution of the schemes for different numbers of iterations n. The number of iterations for Figure 1a is $n = 200$, for Figure 1b is $n = 400$, for Figure 1c is $n = 600$, and for Figure 1d is $n = 800$. These figures illustrate the shock wave propagation for the first-order Godunov schemes. The same numbers of iterations are used for the next figures: $n = 200$ for Figure 2a, $n = 400$ for Figure 2b, $n = 600$ for Figure 2c, and $n = 800$ for Figure 2d. These figures display the rarefaction wave propagation for the first-order Godunov schemes. In each of these subfigures, we investigate three schemes for $\Lambda = -1, \Lambda = 0$, and $\Lambda = 1$ representing SAdS, Schwarzschild, and SdS spacetimes, respectively. As a remark, for the numerical implementation, transmissive boundary conditions are chosen and r is taken in $[0.1, 1]$ with $m = 0.05$. From these graphs we observe that the numerical solution for the particular case $\Lambda = -1$, represented by the red curve, moves faster than the particular cases $\Lambda = 0$ and $\Lambda = 1$, represented by the green curve and the blue curve, respectively. This outcome can also be verified by plugging $\Lambda = -1, 0, 1$ into the speed term given by (4.4). We also observe that, for all particular cases of $\Lambda = -1, 0, 1$, the solution curves converge. More specifically, we can conclude that the numerical solution for the SAdS geometry converges faster than the SdS and Schwarzschild geometries. The convergence rate is smallest for the SdS geometry among these three geometries.

4.2. Second-order Godunov scheme

In this part, we construct a second-order Godunov-type finite volume scheme for the derived model. We give a summary for the algorithm step by step. Starting by discretizing each cell in finite volume, we attain a profile

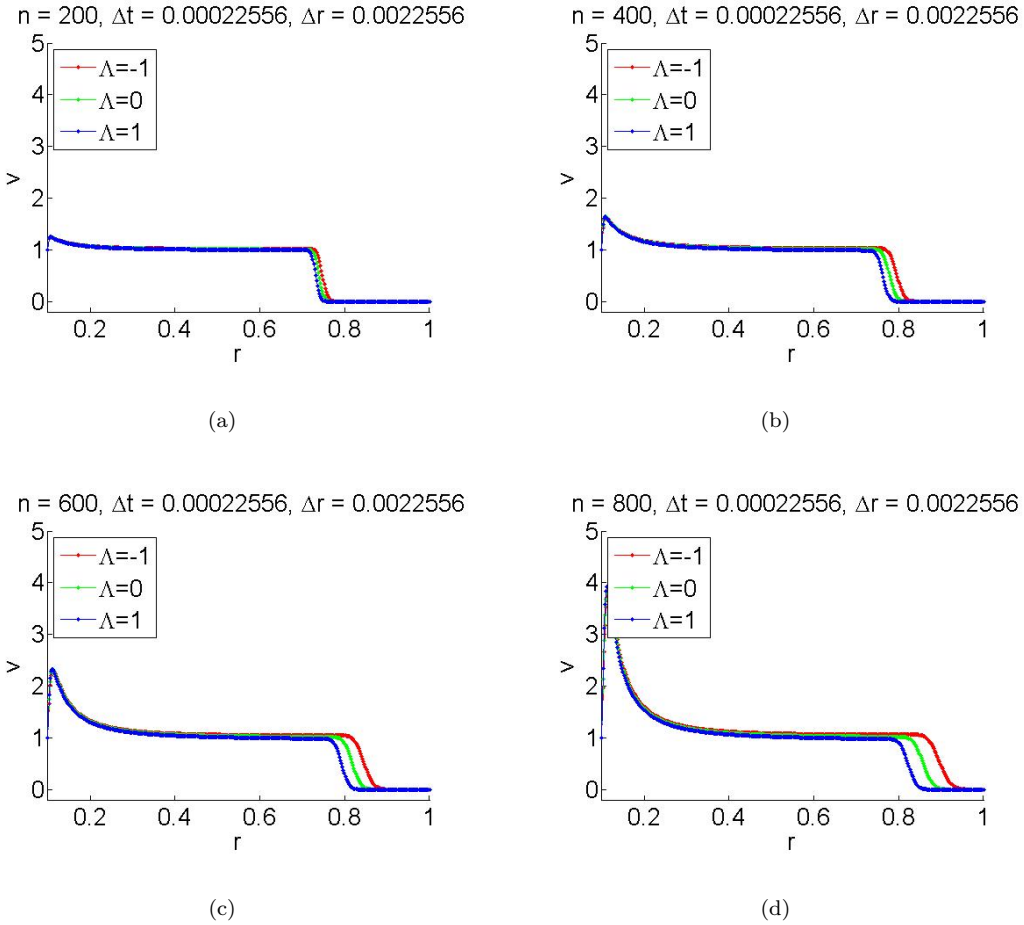

Figure 1. First-order Godunov schemes with shock waves.

construction on the cells. The next step is doing particularization of the Riemann problems at cell interfaces. Then we find the solution for the Riemann problem and do the computation for fluxes on cell interfaces. The final step is determining the variables for the next time stage.

A second-order Godunov-type scheme departs from the first-order Godunov-type scheme in construction of the profile and specification of the Riemann problem. For the equation

$$\partial_t v + \partial_r f(v, r) = 0,$$

a first-order scheme can be converted to a second-order method by proceeding to the cell-boundary values, which are used in the numerical flux functions, to decide the intermediate time level $t^{n+1/2} = (t^n + t^{n+1})/2$. In other words, the second-order Godunov scheme is obtained from the edge-boundary values of the reconstructed profile proceeded by a half time step. The article by Van Leer [9] and the book by Guinot [5] are referred to for construction of the algorithm to the second-order Godunov method.

The model is investigated with a single shock and rarefaction for an initial function considering the Godunov scheme with a local Riemann problem for each grid cell depending on three particular cases of

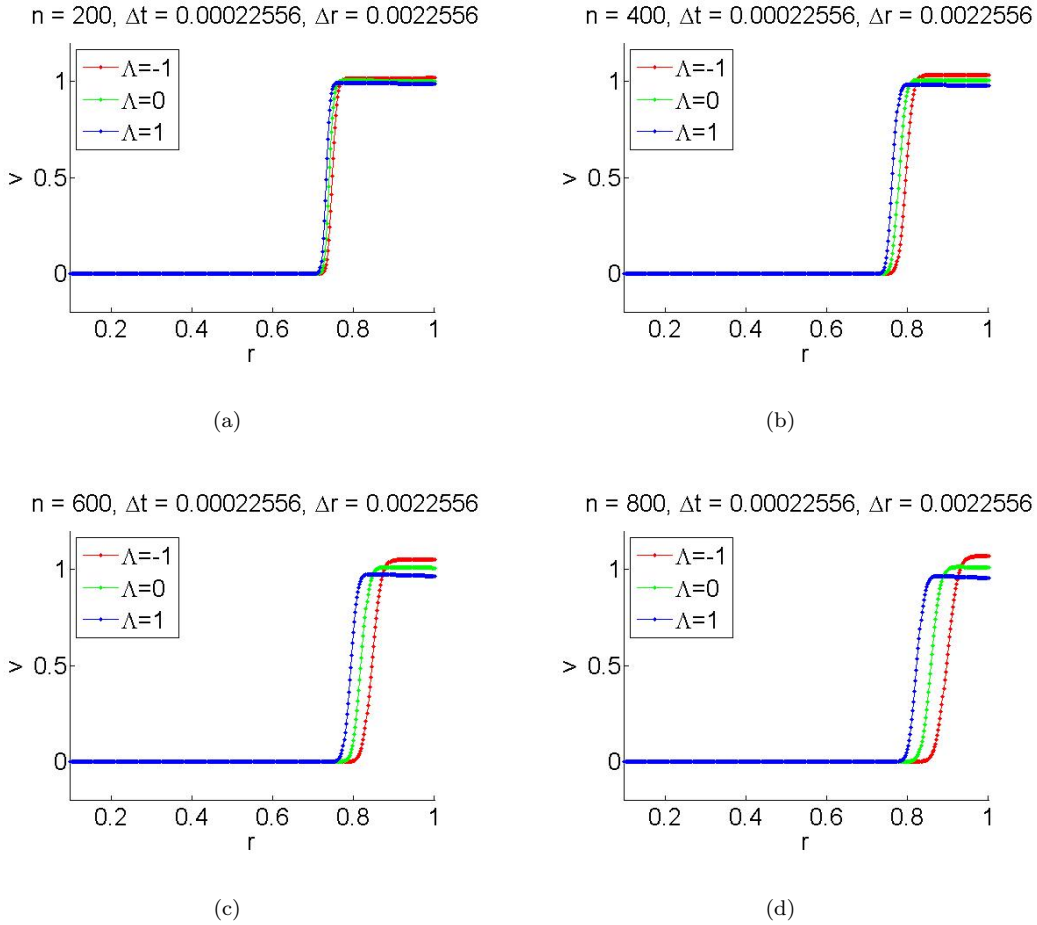

Figure 2. First-order Godunov schemes with rarefaction waves.

cosmological constant Λ. The finite volume scheme for the model (4.1) is given by

$$v_{j\pm1/2}^{n+1/2} = v_{j\pm1/2}^{n} - \frac{\Delta t}{2\Delta r}(b_{j+1/2}^{n} g_{j+1/2}^{n} - b_{j-1/2}^{n} g_{j-1/2}^{n}) + \frac{\Delta t}{2} S_{j\pm1/2}^{n}, \tag{4.5}$$

$$v_{j}^{n+1} = v_{j}^{n} - \frac{\Delta t}{\Delta r}(b_{j+1/2}^{n+1/2} g_{j+1/2}^{n+1/2} - b_{j-1/2}^{n+1/2} g_{j-1/2}^{n+1/2}) + \Delta t S_{j}^{n+1/2}, \tag{4.6}$$

with

$$t^{n+1/2} = (t^{n} + t^{n+1})/2.$$

Here the terms in (4.5) and (4.6) are

$$b_{j\pm1/2}^{n+1/2} = 1 - \frac{2m}{(r_{j\pm1/2}^{n+1/2})} - \frac{\Lambda (r_{j\pm1/2}^{n+1/2})^2}{3},$$

$$g_{j-1/2}^{n+1/2} = f(v_{j-1}^{n+1/2}, v_{j}^{n+1/2}), \qquad g_{j+1/2}^{n+1/2} = f(v_{j}^{n+1/2}, v_{j+1}^{n+1/2}),$$

with the source term

$$S_j^{n+1/2} = \frac{m(v_j^{n+1/2})^2}{(r_j^{n+1/2})^2} - \frac{\Lambda r_j^{n+1/2}(v_j^{n+1/2})^2}{3} - \frac{m}{(r_j^{n+1/2})^2} + \frac{\Lambda r_j^{n+1/2}}{3}.$$

The flux function $f(v_1, v_2)$ has already been defined in (4.3). The speed term is

$$1 - \frac{2m}{(r_{j\pm1/2}^{n+1/2})} - \frac{\Lambda(r_{j\pm1/2}^{n+1/2})^2}{3}, \tag{4.7}$$

and for the stability condition, we select Δt and Δr so that

$$\frac{\Delta t}{\Delta r}\max_j\Big|1 - \frac{2m}{(r_{j\pm1/2}^{n+1/2})} - \frac{\Lambda(r_{j\pm1/2}^{n+1/2})^2}{3}\Big| \leq 1.$$

The implementation of the second-order Godunov scheme is based on the structure given above and presented in Figures 3 and 4. Each of these figures consists of four subfigures displaying the time evolution of the schemes for different numbers of iterations n. The number of iteration for Figure 3a is $n = 200$, for Figure 3b is $n = 400$, for Figure 3c is $n = 600$, and for Figure 3d is $n = 800$. These figures illustrate the shock wave propagation for the second-order Godunov schemes. Finally, to display the rarefaction wave propagation for the second-order Godunov schemes, the same iteration numbers are used. That is, $n = 200$ for Figure 4a, $n = 400$ for Figure 4b, $n = 600$ for Figure 4c, and $n = 800$ Figure 4d. In each of these subfigures, we investigate three schemes for $\Lambda = -1, \Lambda = 0$, and $\Lambda = 1$ representing SAdS, Schwarzschild, and SdS spacetimes, respectively. The number of iterations and the values of r and m are taken the same as in the first-order case. From these graphs we observe that the numerical solution for the particular case $\Lambda = -1$, represented by the red curve, shifts faster than the cases $\Lambda = 0$ and $\Lambda = 1$, represented by the green curve and the blue curve, respectively. This outcome can also be proven by putting $\Lambda = -1, 0, 1$ into the speed term given by (4.7). The solution curves for all particular cases of Λ are convergent, which demonstrates the efficiency and robustness of the scheme. It is again possible to conclude that the numerical solution for the SAdS geometry converges faster than the SdS and Schwarzschild geometries. Once more, the convergence is slowest for the SdS geometry.

4.3. Comparison of first- and second-order schemes

We investigated shock and rarefaction wave propagations for our model with different possible values of the cosmological constant Λ by using the first- and second-order Godunov-type schemes. The numbers of iterations and the values of m and r are fixed for each experiment. One of the more significant findings to emerge from the numerical experiments is that changing the order of the scheme made no significant difference to the results. We obtained almost the same outcomes for the same inputs from the first- and second-order schemes for each particular case, which supports the consistency of numerical results. Furthermore, in each of these experiments, it is observed that the numerical solution for the SAdS geometry converges faster than the SdS and Schwarzschild geometries.

4.4. Summary

An original hyperbolic model that describes the propagation and interactions of shock waves on the SdS and SAdS spacetimes is attained in this paper. We begin with derivation of the relativistic Euler equations on these

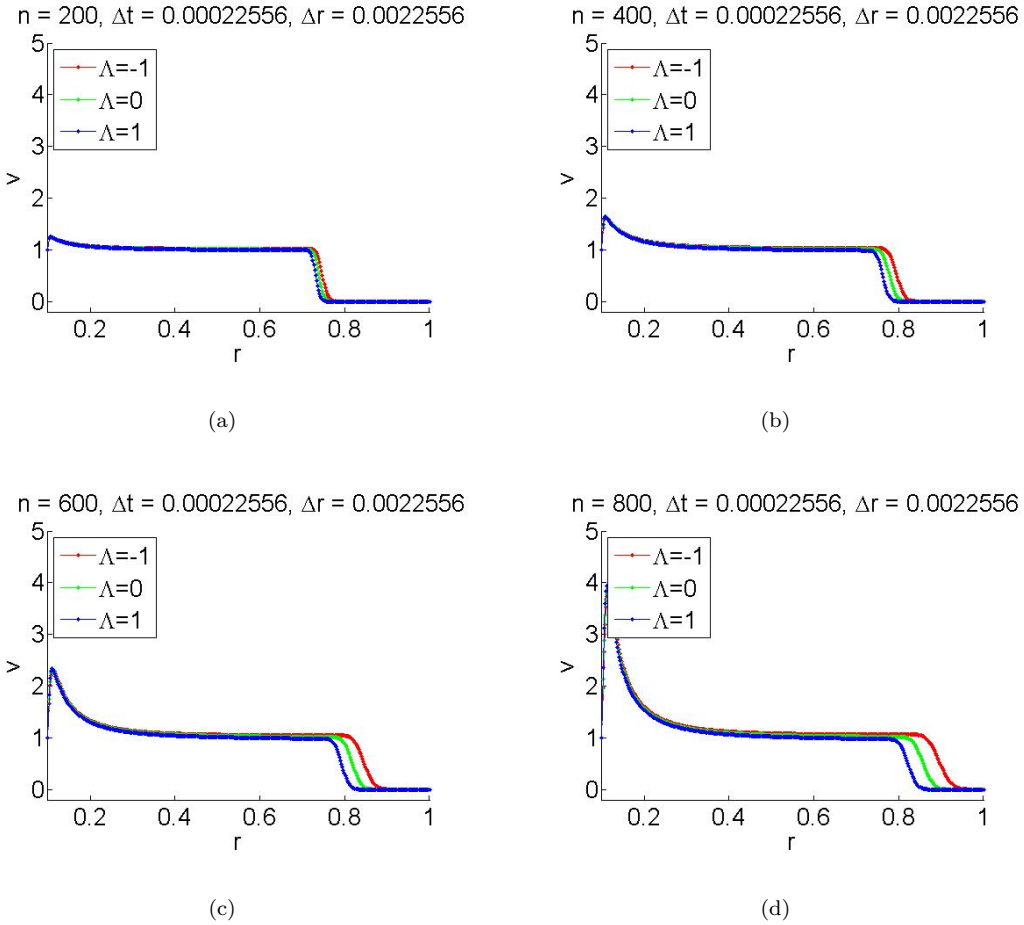

Figure 3. Second-order Godunov schemes with shock waves.

curved backgrounds and impose a vanishing pressure to the energy-momentum tensor for perfect fluids. The pressureless Euler equations yield model (2.13), which involves a cosmological constant factor Λ. According to the sign of Λ, the background geometries become the SdS, SAdS, or Schwarzschild spacetimes. The numerical illustrations are taken into account for these spacetimes separately. As a result, we have the following remarks:

- The findings of this work support those of earlier studies on spacetimes.
- The numerical tests illustrate the convergence, efficiency, and robustness of the proposed scheme on the SdS and SAdS backgrounds.
- This study strengthens the idea that the finite volume scheme is consistent with the conservative form of our model, which yields correct computations of weak solutions containing shock waves, which is a common property shared by the models obtained on the Schwarzschild, FLRW, and de Sitter spacetimes.
- We attain almost the same outcomes for the first- and second-order Godunov schemes for each particular case, which supports the consistency of numerical results.
- The results of this research confirm the idea that the classical (nonrelativistic) Burgers equation can be

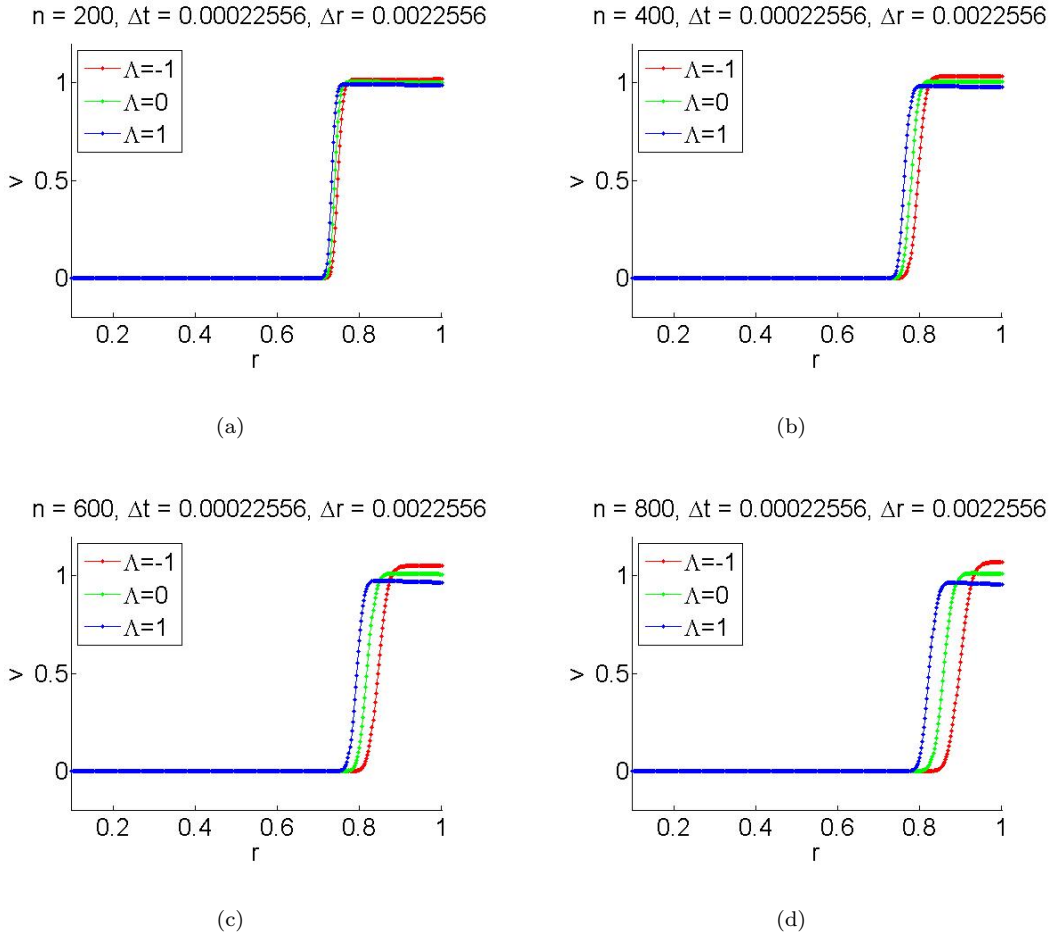

Figure 4. Second-order Godunov schemes with rarefaction waves.

recovered from the derived model, which is a common property shared by relativistic equations. Indeed, for $\Lambda = m = 0$, the model gives exactly the classical Burgers equation.

- Numerical solutions for $\Lambda = -1, 0, 1$ are compared. The solution curve corresponding to $\Lambda = -1$ converges faster than the solution curve corresponding to $\Lambda = 0$ and $\Lambda = 1$. This trait can be verified by observing that the characteristic speed in equations (4.4) and (4.7) is increased by negative values of Λ. Thus, we conclude that the case $\Lambda = -1$ for the solution curves of both first- and second-order finite volume schemes shifts faster than the cases $\Lambda = 0$ and $\Lambda = 1$. In other words, we have faster convergence in the SAdS geometry than the SdS and Schwarzschild geometries.

Acknowledgment

The second author was supported by the Rectorate of Middle East Technical University (METU) through Project BAP-01-01-2016-007.

References

[1] Amorim P, LeFloch PG, Okutmustur B. Finite volume schemes on Lorentzian manifolds. Comm Math Sc 2008; 6: 1059-1086.

[2] Ceylan T, LeFloch PG, Okutmustur B. The relativistic Burgers equation on a FLRW background and its finite volume approximation. arXiv: 1512.08142v1.

[3] Ceylan T, Okutmustur B. Relativistic Burgers equation on a de Sitter background. Derivation of the model and finite volume approximations. International Journal of Pure Mathematics 2015; 2: 21-29.

[4] Ceylan T, Okutmustur B. Finite volume method for the relativistic Burgers model on a $(1+1)$-dimensional de Sitter spacetime. Math Comput Appl 2016; 21: 16.

[5] Guinot V. Godunov-Type Schemes: An Introduction for Engineers. Amsterdam, the Netherlands: Elsevier, 2003.

[6] LeFloch PG, Makhlof H, Okutmustur B. Relativistic Burgers equations on a curved spacetime. Derivation and finite volume approximation. SIAM J Num Anal 2012; 50: 2136-2158.

[7] LeFloch PG, Okutmustur B. Hyperbolic conservation laws on spacetimes. A finite volume scheme based on differential forms. Far East J Math Sci 2008; 31: 49-83.

[8] LeVeque RJ. Finite Volume Methods for Hyperbolic Problems. Cambridge, UK: Cambridge University Press, 2002.

[9] Van Leer B. On the relation between the upwind-differencing schemes of Godunov, Engquist-Osher and Roe. SIAM J Sci Stat Comput 1984; 5: 1-20.